

Redox Dysregulation Affects the Ventral But Not Dorsal Hippocampus: Impairment of Parvalbumin Neurons, Gamma Oscillations, and Related Behaviors

Pascal Steullet,^{1*} Jan-Harry Cabungcal,^{1*} Anita Kulak,^{1*} Rudolf Kraftsik,² Ying Chen,³ Timothy P. Dalton,⁴ Michel Cuenod,¹ and Kim Q. Do¹

¹Department of Psychiatry, Center for Psychiatric Neuroscience, Centre Hospitalier Universitaire Vaudois and University of Lausanne, 1008 Prilly-Lausanne, Switzerland, ²Department of Cell Biology and Morphology, University of Lausanne, 1005 Lausanne, Switzerland, ³Department of Pharmaceutical Sciences, School of Pharmacy, University of Colorado at Denver, Aurora, Colorado 80045, and ⁴Department of Environmental Health, Center for Environmental Genetics, University of Cincinnati Medical Center, Cincinnati, Ohio 45267-0056

Elevated oxidative stress and alteration in antioxidant systems, including glutathione (GSH) decrease, are observed in schizophrenia. Genetic and functional data indicate that impaired GSH synthesis represents a susceptibility factor for the disorder. Here, we show that a genetically compromised GSH synthesis affects the morphological and functional integrity of hippocampal parvalbumin-immunoreactive (PV-IR) interneurons, known to be affected in schizophrenia. A GSH deficit causes a selective decrease of PV-IR interneurons in CA3 and dentate gyrus (DG) of the ventral but not dorsal hippocampus and a concomitant reduction of β/γ oscillations. Impairment of PV-IR interneurons emerges at the end of adolescence/early adulthood as oxidative stress increases or cumulates selectively in CA3 and DG of the ventral hippocampus. Such redox dysregulation alters stress and emotion-related behaviors but leaves spatial abilities intact, indicating functional disruption of the ventral but not dorsal hippocampus. Thus, a GSH deficit affects PV-IR interneuron's integrity and neuronal synchrony in a region- and time-specific manner, leading to behavioral phenotypes related to psychiatric disorders.

Introduction

A hallmark of the pathology of schizophrenia is an alteration of the GABAergic system in prefrontal cortex (PFC) (Lewis et al., 2005) and hippocampus (Zhang and Reynolds, 2002). This includes a reduction of glutamic acid decarboxylase 67 (GAD-67) and the calcium-binding protein parvalbumin (PV) in fast-spiking interneurons (FSIs) (Hashimoto et al., 2003). These FSIs control the output of principal neurons and are necessary for the generation of γ neuronal synchrony that facilitates information processing and transfer within and between brain regions during cognitive tasks (Bartos et al., 2007; Fries et al., 2007; Sohal et al., 2009). Such γ oscillations are reduced in schizophrenia patients during impaired cognitive tasks (Cho et al., 2006; Uhlhaas et al., 2008). This suggests that abnormality in synchronized neuronal activity driven by FSI is a core feature of this disorder.

Recently, it was shown that superoxide overproduction causes the decrease in PV expression in a NMDA receptor (NMDAR) hypofunction model of schizophrenia (Behrens et al., 2007), suggesting that redox dysregulation could affect PV FSI. Elevated

oxidative stress and anomalies in antioxidant systems are found in schizophrenia (Do et al., 2009b), including diminution of brain levels of glutathione (GSH) (Do et al., 2000), the major intracellular antioxidant and redox regulator. While elevated oxidative stress participates in the cellular damage in various neurodegenerative diseases but appears to be a downstream consequence of other primary causes (Valko et al., 2007), a genetic defect in GSH synthesis could be at the origin of the failure of antioxidant defenses in schizophrenia. Both catalytic (GCLC) and modifier (GCLM) subunits of the glutamate cysteine ligase (GCL), the rate-limiting enzyme of GSH synthesis, have been associated with the illness (Tosic et al., 2006; Gysin et al., 2007). Polymorphisms of trinucleotide repeats on the GCLC gene are associated with reduced enzyme activity and GSH levels and confer a high risk for schizophrenia (Gysin et al., 2007). This suggests that dysfunctional regulation of GSH synthesis contributes to the pathology in high-risk genotype patients and selectively impairs development and maturation of structures highly sensitive to oxidative stress. Moreover, several environmental risk factors for schizophrenia lead to increased oxidative stress, alteration of antioxidant systems (Do et al., 2009a), and often permanently decreased PV expression in PFC and/or hippocampus (Dell'Anna et al., 1996; Harte et al., 2007; Meyer et al., 2008). Thus, redox dysregulation could be one causal factor for the dysfunction of the GABAergic system in schizophrenia.

Here, we investigated whether a compromised GSH synthesis affects PV FSI and γ oscillations in the hippocampus. We used GCLM knock-out mice, which have low GSH levels in all organs

Received Aug. 6, 2009; revised Nov. 26, 2009; accepted Dec. 29, 2009.

This work was supported by the Swiss National Science Foundation Grant 31-116689 (to K.Q.D.), "Loterie Romande," and Alamaya Foundation. We thank Adeline Cottier for her technical assistance, Suzie Lavoie for her help on mice management, Fulvio Magara for his support in relation to the mice and behavioral experiments, and Cristina Marquez for her advice on behavioral experiments.

*P.S., J.-H.C., and A.K. contributed equally to this work.

Correspondence should be addressed to Kim Q. Do at the above address. E-mail: kim.do@chuv.ch.

DOI:10.1523/JNEUROSCI.3857-09.2010

Copyright © 2010 the authors 0270-6474/10/302547-12\$15.00/0

including brain (Yang et al., 2002). Results show that the ventral (VH) but not dorsal hippocampus (DH) is highly vulnerable to such redox dysregulation. This is further supported by the fact that mice with a GSH deficit show inadequate responses to stress and fear but have intact spatial learning and spatial memory.

Materials and Methods

Animals. *GCLM* $-/-$ mice were backcrossed with C57BL/6J mice over >10 generations. Mice were housed under a 12 h light/dark cycle in groups of 3–5 individuals per cage. *GCLM* $-/-$ mice were compared to $+/+$ littermates. All experiments were performed in accordance with the guidelines outlined in the *Guide for the Care and Use of Laboratory Animals* and approved by the Local Veterinary Office.

Immunohistochemistry and quantification. Male mice (20 d, 40 d, and 4–6 months old) were anesthetized, perfused, and their brains fixed as described previously (Cabungcal et al., 2006). Coronal and horizontal frozen sections (50 μ m) were used to investigate the DH and VH, respectively. These slices were immunolabeled for PV, calbindin (CB), and calretinin (CR) as described by Cabungcal et al. (2006). The density of PV, CB, and CR-IR cells (cell bodies) was quantified in the different subregions of the hippocampus (CA1, CA3, and DG) using the Stereo- Investigator 7.5 software (MBF Bioscience). Each stereological investigation started at low magnification with the identification of the boundaries of the region of interest (ROI) on two sections from each animal. Boundaries between the hippocampal regions were traced considering the defined cytoarchitectonic areas of CA1, CA3, and DG (i.e., making use of differences in the regional distribution of certain subsets of neurons) (Oleskevich et al., 1989) (supplemental Fig. 1, available at www.jneurosci.org as supplemental material). To ensure that CA1 and CA3 did not overlap and were isolated from each other, an intermediate zone was created between the two regions. CA1 and CA3 ROI in a PV-IR section were also cross-checked with the consecutive calbindin-IR section (supplemental Fig. 2, available at www.jneurosci.org as supplemental material) from the same animal to verify regional boundary. An optical dissector (counting box), within the section thickness and a sampling frame adapted for each region, was used to analyze and count neurons (West et al., 1991; West, 2002; Schmitz and Hof, 2005). The optical dissector boxes (40 \times 40 μ m with a depth of 15 μ m) were systematically placed by the program in each sampling frame starting from a random point inside the ROI of the hippocampus (supplemental Fig. 1, available at www.jneurosci.org as supplemental material). Counting was performed using higher magnification (\times 40 objective). Immunoreactive cells were counted when they were in focus at the surface of the box until out of focus at 15 μ m depth of the counting box. A 5 μ m guard zone was used to avoid artifacts that can be influenced by tissue shrinkage from immunopreparation. Since CA1, CA3, and DG differed in their size, the volume of brain sections analyzed was not equal for each region. In VH, 24 counting frames were used to quantify CA3, 29 for DG, while quantification in CA1 only required 23 frames. In DH, 27 counting frames were used to quantify CA1 and CA3, while quantification in DG required 34 frames. For more details on design stereology, see Schmitz and Hof (2005) and West (1999). The mean numbers of PV, CB or CR-IR cells per unit volume in each of the hippocampal regions were compared between the two genotypes using Kruskal–Wallis tests.

Immunofluorescence staining, confocal microscopy, and image analysis. Oxidative stress was visualized using an antibody against 8-oxo-7,8-dihydro-20-deoxyguanosine (8-Oxo-dG), a DNA adduct formed by the reaction of OH radicals with the DNA guanine base (Kasai, 1997). The same sections were also immunolabeled for DAPI and PV. Briefly, the tissue sections were incubated with PBS plus Triton X-100 0.3% plus sodium azide (1 g/L) containing 2% normal horse serum, followed by a 48 h incubation with rabbit polyclonal anti-PV (1:2500; Swant) and mouse monoclonal anti-8-oxo-dG (1:350; AMS Biotechnology) 1 $^{\circ}$ antibodies. The sections were washed several times before the binding of antibodies was visualized with either fluorescent 2 $^{\circ}$ antibody conjugate, goat anti-mouse IgG (1:300; Alexa Fluor 488; Invitrogen) or anti-rabbit IgG (1:300; CY3; Millipore Bioscience Research Reagents). Sections were counterstained with 100 ng/ml DAPI (4'-6-diamidino-2-phenylindole;

Vector Laboratories). Sections were visualized and processed with a Zeiss confocal microscope equipped with \times 10 and \times 20 Plan-NEOFLUAR objectives. All peripherals were controlled with LSM 510 software (Zeiss). Z-stacks of 9 images (with a 2.97 μ m interval) were scanned (1024 \times 1024 pixels) for analysis in IMARIS 6.2 software (Bitplane). All images of Z-stacks were filtered using a Gaussian filter to remove background noise and sharpen cell profile contours. ROI, defined in the same procedure to those illustrated in supplemental Figure 1 (available at www.jneurosci.org as supplemental material), were created in CA1, CA3, and DG. Each ROI was masked throughout the Z-stacks to isolate regional subvolumes of the brain to be analyzed. In the subvolumes of CA1, CA3, and DG, 8-Oxo-dG labeling (mean fluorescent intensity and number of voxels stained) was quantified using the Coloc module of Imaris 6.2 program. Fluorescent intensity (arbitrary unit) and number of labeled voxels in each of the hippocampal regions were compared between the two genotypes using Kruskal–Wallis tests.

Electrophysiology recording and analysis. Adult male mice (4–6 months old) were first anesthetized under isoflurane and decapitated. Brains were quickly removed, hemisectioned, and hippocampal slices (350 μ m thick) prepared with a vibroslicer in aerated artificial CSF (ACF) as follows (in mM): 220 sucrose, 2 KCl, 4 MgCl₂, 0.5 CaCl₂, 1.2 NaH₂PO₄, 26 NaHCO₃, 10 glucose; pH 7.4. Horizontal hemisphere sections were used to make transverse slices of the VH. Transverse slices of the DH were achieved via \sim 30 $^{\circ}$ tilted coronal hemisphere sections. Slices were maintained in interface chambers superfused with aerated ACF as follows (in mM): 125 NaCl, 3 KCl, 2 MgCl₂, 1.2 CaCl₂, 1.2 NaH₂PO₄, 26 NaHCO₃, 10 glucose; pH 7.4 at 30–31 $^{\circ}$ C for at least 90 min before starting electrophysiological recordings.

Gamma oscillations were induced with 200 nM kainate and recorded in the CA3 stratum pyramidalis with ACF-filled electrode (\sim 1 M Ω). Signals were bandpass filtered at 1–1000 Hz and digitized at 5 kHz. For each slice, 60 s recording was used for power spectrum analysis using the Welch method (IgorPro6 WaveMetrics). The power density of the β/γ oscillations was defined as the integral of the power spectrum between 20 and 80 Hz. The power of β/γ oscillations in *GCLM* $-/-$ and $+/+$ mice was compared using Mann–Whitney test. Peak frequency of β/γ oscillations in *GCLM* $-/-$ and $+/+$ mice was compared with *t* test.

Extracellular responses evoked by electric stimulation of the Schaffer collaterals were recorded with ACF-filled electrodes (\sim 5 M Ω) in the stratum pyramidalis of the CA3 (for the CA3 recurrent pathway), or in the stratum radiatum and stratum pyramidalis of the CA1 (for the Schaffer collaterals–CA1 pathway). The stimulation electrode was made of two twisted Teflon-coated platinum/iridium wires. Stimulation consisted of 100 μ s bipolar current pulses generated by a stimulus isolator (model 2200, A-M Systems) and driven by a computer software (WinWCP). Signals (0.3–3000 Hz) were amplified with a Grass preamplifier (model P15, Grass Instruments) and digitized via a Digidata 1300 (Molecular Devices). Experiments were initiated when stability of responses evoked by a 0.033 Hz baseline stimulation was maintained for \sim 15 min. Responses to a series of single electric stimulations ranging from 10 to 300 μ A were thus recorded. Paired-pulse stimulations (stimulus interval ranging from 10 to 100 ms) at an intensity evoking \sim 40% of maximal population spike (PS) were used to examine paired-pulse inhibition in the stratum pyramidalis of CA1. Paired-pulse inhibition was defined as the ratio between the amplitude of the PS evoked by the second stimulus (PS2) and the amplitude of the PS induced by the first stimulus (PS1). Quantification of the field EPSPs (fEPSPs) was based on their initial slope (when recorded in CA1 stratum radiatum) or on their amplitude (when recorded in CA3 stratum pyramidalis). To estimate the effect of genotype on fEPSPs or PS, a General linear model with genotype as factor and fEPSPs or PS at different stimulus intensities as repeated measure was applied. To estimate the effect of genotype on paired-pulse inhibition, a General linear model with genotype as factor and the ratio PS2/PS1 for different stimulus intervals as repeated measure was applied.

GSH measurements. Total GSH levels (reduced and oxidized forms) were quantified in different brain structures (cortex, hippocampus, striatum, midbrain, cerebellum) as described previously (Steullet et al., 2008). GSH measurement in VH and DH was performed on parts of the DH and VH that were dissected out from frozen coronal and horizontal

Table 1. Deficit in GSH levels in different brain structures of 35- to 40-d-old *GCLM* $-/-$ relative to $+/+$ mice

	Cortex	Hippocampus	Striatum	Midbrain	Cerebellum
Percent GSH in <i>GCLM</i> $-/-$ relative to $+/+$ mice	36 ± 2	32 ± 1	32 ± 2	24 ± 2	26 ± 3

Brain total GSH deficit in *GCLM* $-/-$ mice. The GSH deficit is expressed as percent of GSH levels in *GCLM* $-/-$ mice relative to those in $+/+$ mice. GSH measurements have been performed in at least four mice per genotype and per age. Data are presented by mean ± SEM.

Table 2. Deficit in GSH levels in brain (anterior cortex) of *GCLM* $-/-$ relative to $+/+$ mice at different ages

	5–6 days old	16–20 days old	35–40 days old	3 months old
Percent GSH in <i>GCLM</i> $-/-$ relative to $+/+$ mice	17 ± 2	31 ± 1	31 ± 3	28 ± 2

Brain total GSH deficit in *GCLM* $-/-$ mice. The GSH deficit is expressed as percent of GSH levels in *GCLM* $-/-$ mice relative to those in $+/+$ mice. GSH measurements have been performed in at least four mice per genotype and per age. Data are presented by mean ± SEM.

brain slices, respectively. GSH levels in VH and DH were compared using paired sample *t* test, where each pair was from the same mouse.

Behavioral tests and analysis. Adult male *GCLM* $-/-$ and $+/+$ mice were subjected to the following behavioral tests: object recognition, rewarded alternation in a T-maze, spatial reference learning and memory in a water maze, elevated plus maze, novelty-suppressed feeding, light/dark transition, and delay fear conditioning.

Object recognition. The mouse was habituated for 10 min to the arena, which consisted of a gray nontranslucent Plexiglas arena (50 × 50 × 30 cm) with internal spatial cues on the walls. Five min after the end of this habituation period, the mouse was familiarized to three objects (7–8 cm high, 5 cm wide, differing in texture, material, color, and form) that were arranged in a determined spatial configuration. The familiarization phase consisted of 3 × 10 min sessions interspaced by 5 min intervals. After the third familiarization session and following a retention delay of 10 min, the mouse was placed back into the arena where one of the three objects had been moved to a new location. The animal was given 10 min to explore the novel spatial configuration (test for spatial recognition of objects). Thereafter, the mouse was familiarized to this novel object arrangement during a 10 min session. After this familiarization session and following a retention delay of 10 min, the animal was placed back into the arena where this time one novel object had replaced one of the two objects that were previously not displaced. The animal was given 10 min to explore the novel object (object recognition test). During all delays, mice were placed into a holding cage in which they had *ad libitum* access to food and water. All test sessions were video-recorded. The number of object contacts was quantified after each session. General Linear Model was used for statistical analysis. First, a multivariate analysis with genotype as factor and the number of contacts to each object as dependent measures was performed to estimate the genotype effect and determine whether each object was explored differently by the two genotypes. A two-way ANOVA (genotypes × objects) was then performed. If an object effect was found, *post hoc* one-way ANOVAs with Bonferroni's corrections were run for each genotype to compare the number of contacts at the displaced or novel object with the number of contacts at each of the nondisplaced or familiar objects.

Rewarded alternation task. Mice were maintained on a restricted feeding schedule at 85% of their free-feeding weight throughout the entire test period. Spatial working memory was assessed during a rewarded alternation task in a T-maze consisting of three translucent Plexiglas tunnel arms (30 cm long, 5 cm wide, 7 cm high). Extra-maze visual cues in the room were available to the mice. The start arm contained a sliding door at its distal end, through which a mouse could be released into the maze. On three consecutive days, mice were habituated to run in the maze and consume food rewards (pieces of sweetened nut cereals) placed at 3 cm from the distal end of each of the two goal arms. Testing started on the fourth day and consisted of a total of 32 trials, three trials per day with an intertrial interval of at least 20 min. Each trial was composed of one forced run and one choice run. On a forced run, the mouse was placed into the start arm and was granted access to only the right or left goal arm which was baited; access to the other arm was blocked by a removable white plastic door. Baiting of the arms followed a pseudo-random sequence. The forced run was completed when the mouse had consumed the reward. After a delay of 15 s, which the mouse spent in a

holding cage, the animal was placed back into the start arm for the choice run, during which it had access to both goal arms, but was only rewarded for choosing the previously unvisited arm. Percent of correct choice (unvisited arm) during the choice run was used to evaluate spatial working memory. A General Linear Model with genotype as factor and the percent correct choice during each of the 4 trial blocks as repeated measure was used to determine the genotype effect. A two-way ANOVA (genotypes × blocks) was also performed to test whether the percent of correct choice increased over the successive trial blocks.

Spatial reference learning and memory in a water maze. The water maze consisted of a large gray circular tank (120 cm diameter, 50 cm high) filled with milky water (15 cm depth) held at 26°C (± 1°C). A goal platform (14 × 14 cm), made of clear Plexiglas covered with a white plastic rubber mash, was submerged 0.5 cm below the water surface. Walls surrounding the maze possessed salient extra-maze cues. For each trial, a mouse was placed into the maze at one of four start positions facing the pool wall (pseudo-randomly counterbalanced between trials and days). Mice performed 25 trials, 4 trials per day for 6 d with intertrial intervals of at least 15 min. During the first 12 trials, mice were trained with the hidden goal platform kept in a constant position. Trial 13 served as a probe trial during which the platform was removed. Spatial reference memory during the 60 s probe trial was assessed by measuring the time spent in the goal quadrant relative to adjacent quadrants. For the remaining trials, the goal platform was replaced at a new position to assess reversal learning capacity. Swim trajectories (path, velocity, and distance) were monitored with a video camera and analyzed with Ethovision (Noldus). Latency to find the hidden platform served as index for spatial reference learning. A General Linear Model with genotype as factor and the latency to escape during each of the trial blocks as repeated measure was used to determine the genotype effect. For the probe trial, a multivariate analysis (General Linear Model) with genotype as factor and time spent in each quadrant as dependent measures was performed to estimate the genotype effect. A two-way ANOVA (genotypes × quadrants) was then performed. If a quadrant effect was found, *post hoc* one-way ANOVAs with Bonferroni's corrections were run for each genotype to compare the time spent in the goal quadrant with the time spent in each of the other quadrants.

Elevated plus maze. Mice were acclimated to the room for at least 15 min before testing. The elevated plus maze consisted of white Plexiglas runways (each 30 cm long and 5 cm wide) arranged in form of a plus and positioned 65 cm above the floor. Two opposing runways were protected by black Plexiglas walls (10 cm high; closed arms), while the other two opposing arms had no walls (open arms). All four arms were joined by a center platform (5 × 5 cm). A mouse was placed into the center of the maze facing an open arm, and its behavior was monitored for 10 min using an automated tracking software. Entry frequency into the open and closed arms were recorded. An arm entry was considered when the whole body (tail excluded) of the animal entered a zone. One-way ANOVAs were used to compare entries in open arms and total entries in both open and closed arms in the two genotypes.

Novelty-suppressed feeding. Mice were subjected to a novelty-suppressed feeding conflict paradigm after being food deprived for 23 h. The testing apparatus consisted of a white nontranslucent Plexiglas arena (60 × 40 × 20 cm) with the floor covered by ~2 cm of wooden bedding.

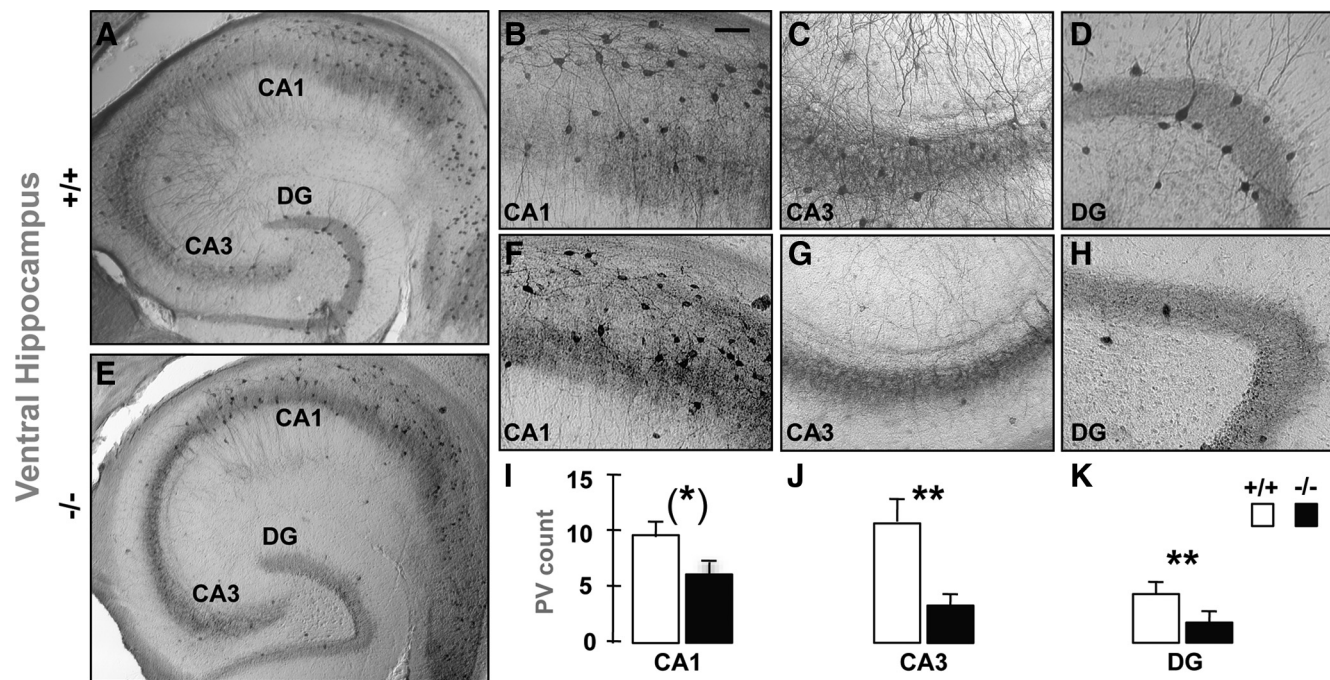


Figure 1. Parvalbumin-immunoreactive (PV-IR) profiles in the ventral hippocampus of adult *GCLM* +/+ (**A–D**) and *GCLM* -/- (**E–H**) mice. Micrographs show horizontal sections of the entire hippocampus (**A, E**), and parts of CA1 (**B, F**), CA3 (**C, G**), and dentate gyrus (DG) (**D, H**), where PV-IR cells are clearly visible. The horizontal sections were taken ~3.5 mm above the interaural line and -6.50 mm bregma. **I–K**, Stereological quantification shows that the number of PV-IR FSI (mean ± SEM) in DG and CA3 is significantly lower in *GCLM* -/- ($n = 7$) than in +/+ ($n = 5$) mice. In CA1, the reduced density of PV-IR FSI in *GCLM* -/- mice is close to significant. ** $p < 0.01$, * $p = 0.051$. Scale bar: 50 μ m.

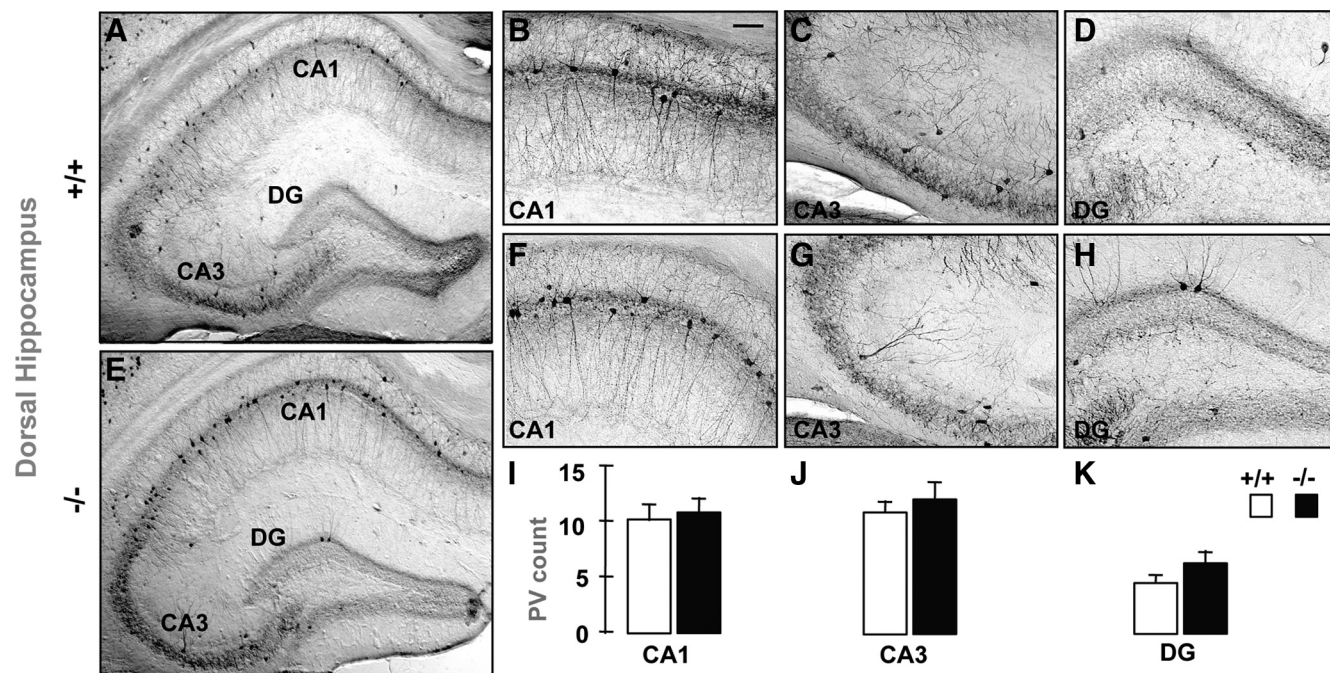


Figure 2. **A–H**, Parvalbumin-immunoreactive (PV-IR) profiles in the dorsal hippocampus of adult *GCLM* +/+ (**A–D**) and *GCLM* -/- (**E–H**) mice. Micrographs show coronal sections of the entire hippocampus (**A, E**), and parts of CA1 (**B, F**), CA3 (**C, G**), and dentate gyrus (DG) (**D, H**) where PV-IR cells are clearly visible. The coronal sections were taken ~-3.1 mm bregma and 5.5 mm above the interaural line. **I–K**, Stereological quantification shows for all subregions that the number of PV-IR FSI (mean ± SEM) does not differ in *GCLM* -/- ($n = 9$) and +/+ ($n = 9$) mice. Scale bar: 50 μ m.

A food pellet was placed on a piece of white filter paper (12 cm diameter) in the center of the arena. A mouse was released in one corner of the arena and allowed to explore for a maximum of 15 min. The latency to approach and start eating the pellet was recorded. As a control for the food uptake motivation of each mouse, the latency to approach and start

eating a pellet introduced in the home cage was also measured. One-way ANOVA was used to compare the feeding latency in the two genotypes.

Light/dark transition. The light/dark transition test was conducted in a two-chamber apparatus. The light chamber (20 × 30 cm) with transparent Plexiglas walls (20 cm high), was open at the top and illuminated by

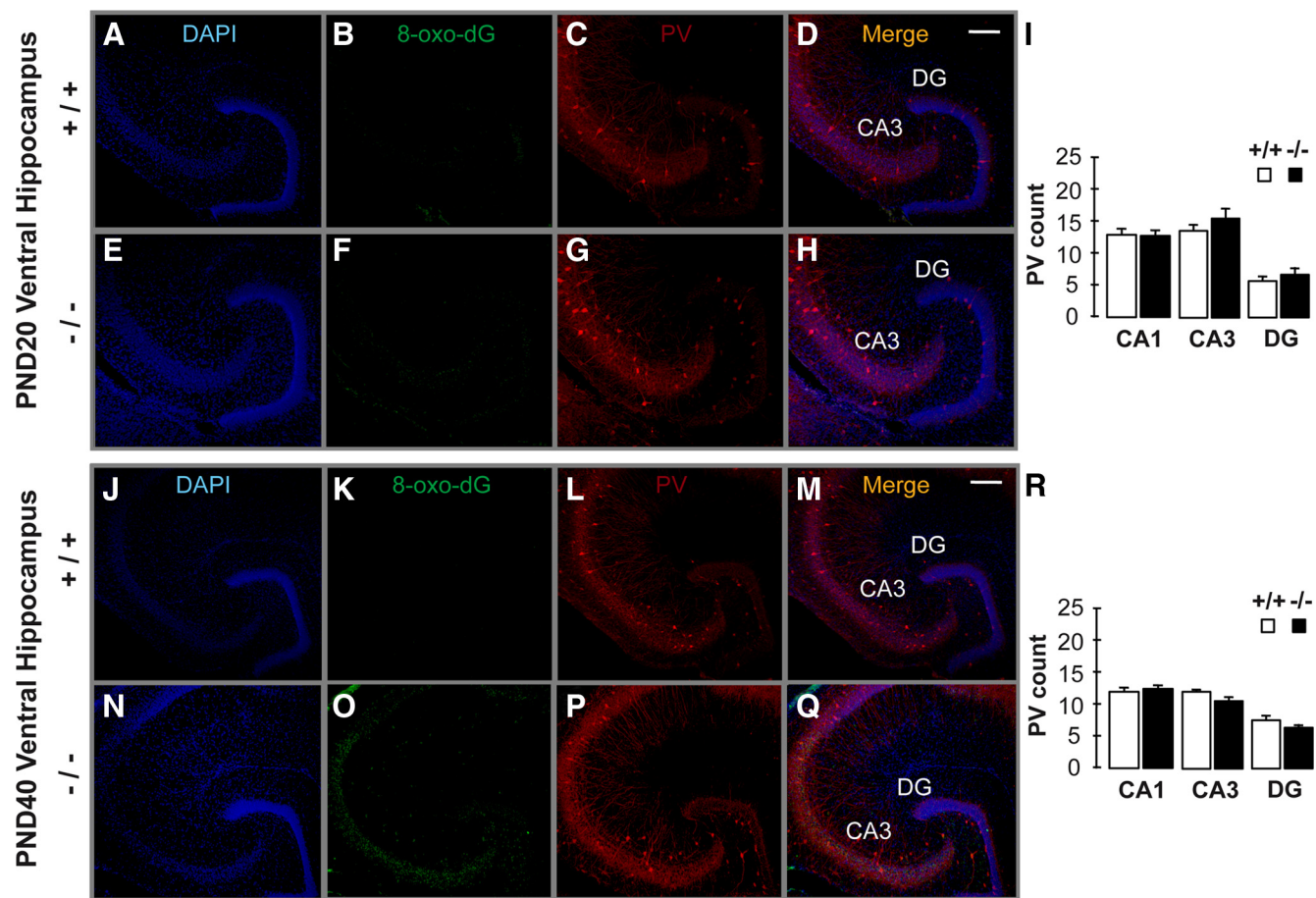


Figure 3. A–R, Localization of oxidative stress and PV-IR profiles in ventral hippocampus of 20-d-old (PND 20) (A–I) and 40-d-old (PND 40) (J–R) *GCLM* +/+ and -/- mice. A, E, J, N, DAPI staining of cell nuclei (blue). B, F, K, O, DNA oxidation as revealed with 8-Oxo-dG labeling (green). (C, G, L, P) PV-IR (red). (D, H, M, Q) Colocalization of the markers. In contrast with the strong 8-Oxo-dG labeling in ventral hippocampus of adult *GCLM* -/- mice (Fig. 4F), 8-Oxo-dG labeling is absent in CA3 and DG of PND 20 mice of both genotypes (B, F). In PND 40 mice, 8-Oxo-dG labeling is significant in CA3 of *GCLM* -/- compared to +/+ mice (K, O). However, 8-Oxo-dG labeling is still much lower in PND 40 than in adult *GCLM* -/- mice (see text for details). I, R, Stereological quantification shows that the number of PV-IR FSI is not significantly reduced in PND 20 and PND 40 *GCLM* -/- compared to corresponding +/+ mice ($n = 5$ for each age and genotype). This contrasts with the reduced density of PV-IR FSI in ventral hippocampus of adult *GCLM* -/- mice (Fig. 1). Scale bar: 200 μ m.

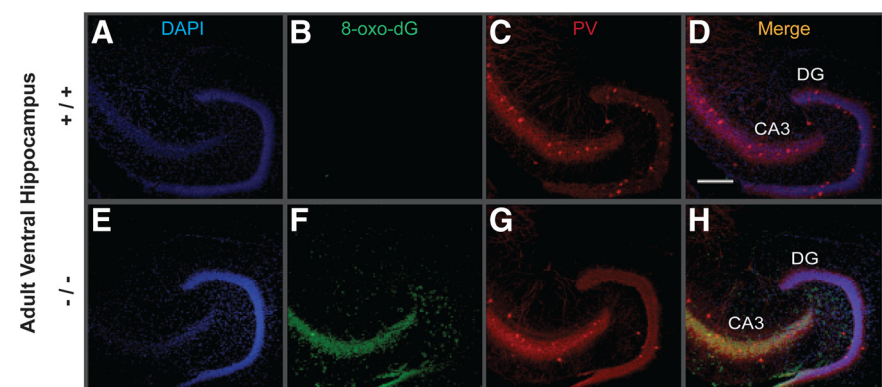


Figure 4. Localization of oxidative stress and PV-IR in DG and CA3 of ventral hippocampus of adult *GCLM* +/+ and -/- mice. A, E, DAPI staining of cell nuclei (blue). B, F, DNA oxidation as revealed with 8-Oxo-dG labeling (green). C, G, PV-IR (red). D, H, Colocalization of the markers. Note the strong 8-Oxo-dG labeling in CA3 and hilar cells annexed to the DG in *GCLM* -/- (F) but not in +/+ (B) mice. A reduction in density of PV-IR FSI (cell bodies) particularly in DG of *GCLM* -/- (G), as compared to +/+ (C) mice, is also observed. Scale bar, 200 μ m.

direct room light. The dark chamber (20 × 15 cm) was surrounded by black Plexiglas walls (20 cm high) and closed at the top with a black plastic lid. A 7.5 × 7.5 cm opening connected the two chambers. A mouse was placed into the light chamber and allowed to freely move between the two chambers for a 15 min period. All test sessions were video recorded.

The number of transitions between the two compartments and the total time spent in the light compartment (after the mouse entered the dark chamber for the first time) were measured. One-way ANOVAs were used to compare the number of transitions and the total time spent in the light compartment by the two genotypes.

Delay contextual and auditory-cued fear conditioning. For conditioning on test day 1, a mouse was placed into the conditioning chamber (20 × 32 × 21 cm, shuttle box, Med Associates) for 9 min. After a 4 min habituation period, a sound (2900 Hz, 85 dB) was presented for 30 s (conditional stimulus, CS). During the last 2 s of the CS, a weak electric footshock (0.35 mA) was delivered (unconditional stimulus, UC). This CS-US pairing was repeated 3 times at 1 min intervals. Contextual fear conditioning was assessed on test day 2, 24 h after the conditioning sessions by placing the mouse again into the conditioning chamber and quantifying the amount of freezing behavior (absence of movement except breathing) during a 9 min period.

Auditory-cued fear conditioning was evaluated on test day 3, 24 h after the contextual fear conditioning test, by placing the mouse into a novel chamber clearly distinct from the conditioning chamber (different wall color and material, absence of metallic mesh on the floor, different illu-

mination). After 4 min of habituation, the conditioned tone was played for 5 min. The amount of freezing during the sound presentation was quantified. A General Linear Model with genotype as factor and activity level before and during the fear conditioning paradigm as repeated measure was used to determine the genotype effect and whether conditioning had an effect on activity level. A General Linear Model with genotype as factor and freezing after each electric shock as repeated measure was also performed to determine the effect of genotype and shock on freezing. The effect of genotype on contextual fear conditioning was estimated using a General linear model with genotype as factor and percent freezing at each minute bin as repeated measure (nine bins corresponding to 9 min stay in the conditioning chamber), followed by *post hoc* one-way ANOVAs at each times bins. Finally the effect of genotype on auditory-cued fear conditioning was estimated using a General linear model with genotype as factor and percent freezing at each minute bin of the tone duration as repeated measure (five bins corresponding to 5 min tone presentation), followed by *post hoc* one-way ANOVAs at each times bins.

Statistical analysis. Statistical tests are given under the description of each method. $p < 0.05$ is considered statistically significant.

Results

Brain GSH deficit in *GCLM* $-/-$ mice

GCLM $-/-$ mice displayed quite similar GSH deficit throughout the brain including hippocampus (Table 1). Total GSH levels in *GCLM* $-/-$ mice were $\sim 30\%$ of those measured in $+/+$ littermates. This GSH deficit remained fairly constant throughout life (Table 2). In young adult $+/+$ mice (4–6 months old), GSH levels in VH (8.4 ± 0.3 nmol GSH/mg protein, mean \pm SEM, $n = 6$) and DH (7.9 ± 0.4 nmol GSH/mg protein, mean \pm SEM, $n = 6$) were not significantly different ($p = 0.097$). In young adult *GCLM* $-/-$ mice however, GSH levels were significantly higher in VH (3.4 ± 0.4 nmol GSH/mg protein, $n = 6$) than in DH (2.7 ± 0.3 nmol GSH/mg protein, $n = 6$) ($p = 0.045$).

Reduced density of PV-IR FSI in VH of *GCLM* $-/-$ mice

The number of PV-IR FSI (Fig. 1), but not CB- and CR-IR interneurons (supplemental Fig. 2, available at www.jneurosci.org as supplemental material), was significantly lower in the VH of young adult *GCLM* $-/-$ compared with $+/+$ mice. The defect in PV was significant in the dentate gyrus (DG) and CA3, but was at the limit of significance in CA1 (Fig. 1, supplemental Table 1, available at www.jneurosci.org as supplemental material). In contrast in DH, number of PV-IR FSI (Fig. 2) (supplemental Table 1, available at www.jneurosci.org as supplemental material) did not differ between genotypes. In 20-d-old mice, when developmental PV expression is almost complete (Dell'Anna et al., 1996), *GCLM* $-/-$ mice did not have a deficit in number of PV-IR FSI in VH (Fig. 3C,G,I). Likewise in mid-adolescent (40-d-old) mice, the density of PV-IR FSI was not significantly different in both genotypes (Fig. 3L,P,R). However in contrast with 20-d-old mice, there was a trend toward a decrease density of PV-IR FSI in the CA3 and DG of mid-adolescent *GCLM* $-/-$ mice. Thus, a chronic deficit in GSH leads to PV-IR FSI impairment in the VH, but not DH, which emerges gradually during adolescence and early adulthood.

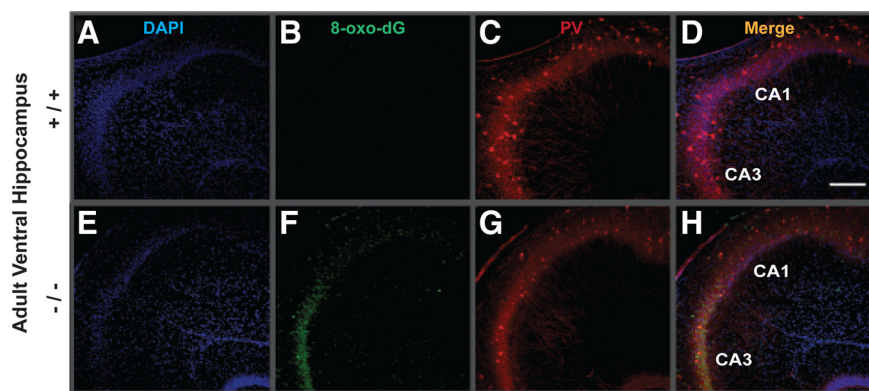


Figure 5. Localization of oxidative stress PV-IR in CA1 and CA3 of ventral hippocampus of adult *GCLM* $+/+$ and $-/-$ mice. **A, E**, DAPI staining of cell nuclei (blue). **B, F**, DNA oxidation as revealed with 8-Oxo-dG labeling (green). **C, G**, PV-IR (red). **D, H**, Colocalization of the markers. 8-Oxo-dG labeling is strong in CA3 and weaker in CA1 of *GCLM* $-/-$ (**F**), but absent in $+/+$ mice (**B**). A reduction of PV-IR FSI in *GCLM* $-/-$ (**G**), as compared to $+/+$ (**C**) mice, is also observed. Scale bar, 200 μm .

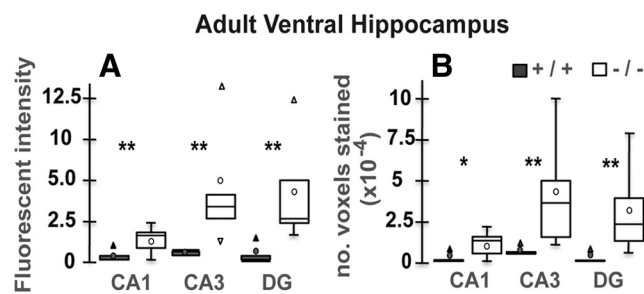


Figure 6. Quantification of oxidative stress using 8-Oxo-dG labeling in ventral hippocampus of adult *GCLM* $+/+$ ($n = 5$) and $-/-$ mice ($n = 5$). **A**, Mean fluorescent intensity of 8-Oxo-dG-labeled voxels (represents level of oxidative stress). The fluorescent intensity is significantly higher in all regions of the ventral hippocampus of *GCLM* $-/-$ compared to $+/+$ mice. **B**, Number of voxels labeled with 8-Oxo-dG (represents the extent of oxidative stress). The number of labeled voxels is significantly higher in all regions of the ventral hippocampus of *GCLM* $-/-$ compared to $+/+$ mice. Note that 8-Oxo-dG labeling (based on mean intensity and number of labeled voxels) is particularly strong in DG and CA3. Data are presented with the quartiles (bar), median (horizontal line inside the bar), mean (circle), and outliers (triangle). ** $p < 0.01$, * $p < 0.05$.

Oxidative stress in VH of *GCLM* $-/-$ mice

To see whether the anomaly of PV-IR FSI in VH was associated with a region-specific increase in oxidative stress, we used an antibody against 8-oxo-7,8-dihydro-20-deoxyguanosine (8-Oxo-dG), a marker for DNA oxidative damage (Kasai, 1997). The VH (Figs. 4, 5, 6) but not DH (Fig. 7) of young adult *GCLM* $-/-$ showed prominent oxidative stress compared to $+/+$ mice. Within the VH of adult *GCLM* $-/-$, 8-Oxo-dG labeling was most prevalent in CA3 and hilus of the DG (Figs. 4, 6) and less pronounced in CA1 (Figs. 5, 6). Such oxidative stress was not observed in VH of 20-d-old *GCLM* $-/-$ mice (Fig. 3B,F). In 40-d-old animals, oxidative stress was significantly higher in ventral CA3 of *GCLM* $-/-$ compared to $+/+$ mice ($p = 0.026$ for 8-Oxo-dG labeling intensity; $p = 0.046$ for number of labeled voxels; $n = 5$ for each genotype), but not in DG (Fig. 3K,O). However, 8-Oxo-dG labeling intensity and number of labeled voxels were respectively 7.5 and 9.1 times lower in ventral CA3 of 40-d-old than in ventral CA3 of adult *GCLM* $-/-$ mice (Fig. 6). This indicates, as with PV-IR FSI, that the VH (CA3 and DG) is particularly vulnerable to oxidative stress and that such redox dysregulation emerges gradually during adolescence.

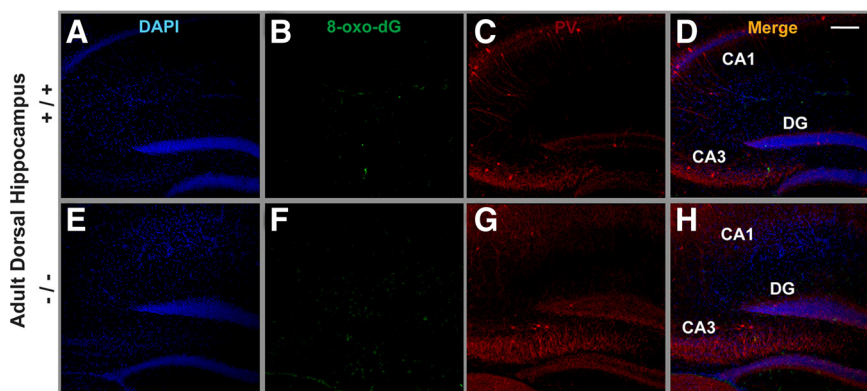


Figure 7. Localization of oxidative stress and PV-IR in dorsal hippocampus of adult *GCLM* *+/+* and *-/-* mice. **A, E**, DAPI staining of cell nuclei (blue). **B, F**, DNA oxidation as revealed with 8-Oxo-dG labeling (green). **C, G**, PV-IR (red). **D, H**, Colocalization of the markers. Note that 8-Oxo-dG labeling is almost absent in both genotypes (**B, F**). This contrasts with the strong 8-Oxo-dG labeling observed in ventral hippocampus of adult *GCLM* *-/-* mice (Fig. 4*F*). The absence of 8-Oxo-dG labeling in dorsal hippocampus of both genotypes was observed systematically in all 5 *GCLM* *-/-* and 5 *+/+* mice investigated. Scale bar, 200 μ m.

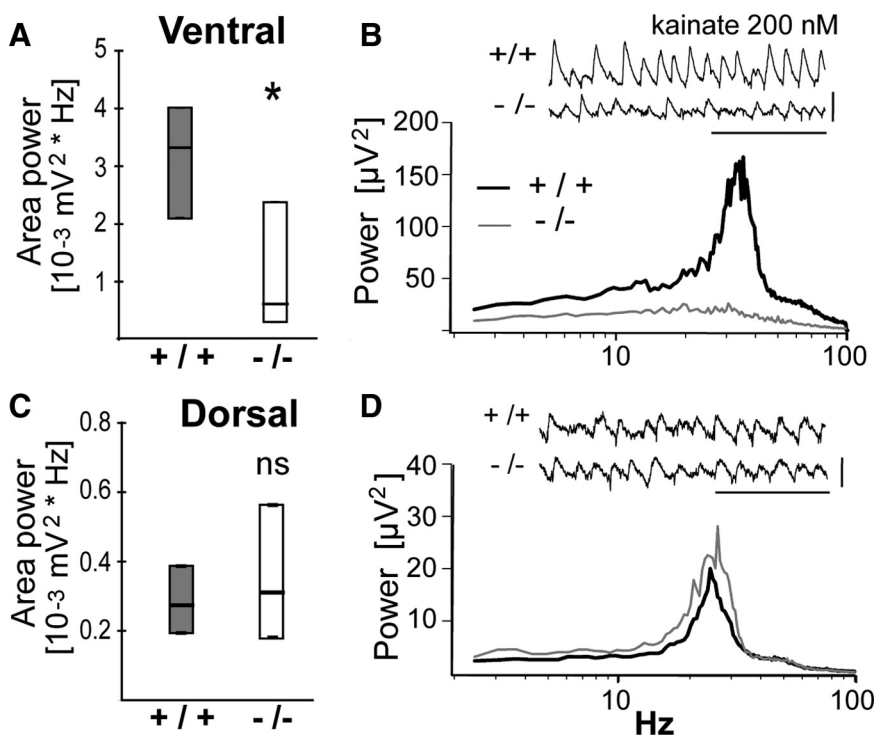


Figure 8. **A, B**, In ventral hippocampus, kainate-induced β/γ oscillations are weaker in *GCLM* *-/-* than *+/+* mice. **A**, Power of oscillations (20–80 Hz) is significantly lower in *GCLM* *-/-* than *+/+* mice. $*p < 0.05$. Data (median and quartiles) are from 13 hippocampus of 9 *+/+* mice and 11 hippocampus of 7 *-/-* mice. **B**, Power spectrum (median) of the traces recorded from ventral hippocampus of *GCLM* *-/-* and *+/+* mice under kainate superfusion. Insert shows a typical trace recorded in ventral hippocampus of each genotype. Horizontal bar: 0.2 s; vertical bar: 0.2 mV. **C, D**, In dorsal hippocampus, kainate-induced β/γ oscillations are not different in *GCLM* *-/-* and *+/+* mice. **C**, Power of oscillations (20–80 Hz) are not significantly different between genotypes (ns). Data (median and quartiles) are from 10 hippocampus of 5 *+/+* mice and 11 hippocampus of 6 *-/-* mice. **D**, Power spectrum (median) of the traces recorded from dorsal hippocampus of *GCLM* *-/-* and *+/+* mice under kainate superfusion. Insert shows a typical trace recorded in dorsal hippocampus of each genotype. Horizontal bar: 0.2 s; vertical bar: 0.1 mV.

Reduced kainate-induced γ oscillations in VH of *GCLM* *-/-* mice

Since PV-IR FSI are necessary for the generation of γ oscillatory synchronization (Sohal et al., 2009), we examined whether the reduced number of PV-IR FSI in VH of adult *GCLM* *-/-* mice was associated with reduced γ oscillations. We quantified γ oscillations

induced by kainate in CA3 of VH and DH slices. In VH, kainate generated significantly less powerful β/γ oscillations (20–80 Hz) in adult *GCLM* *-/-* than in *+/+* mice (Fig. 8*A, B*). The peak frequency of these oscillations was not significantly different in *GCLM* *-/-* (32.2 ± 1.4 Hz) and *+/+* mice (28.7 ± 1.9 Hz). In contrast in DH, the power (Fig. 8*C, D*) and the peak frequency of β/γ oscillations (24.0 ± 0.9 Hz vs 25.3 ± 0.4 Hz) did not differ in *GCLM* *-/-* and *+/+* mice. Thus, a chronic deficit in GSH impairs β/γ oscillations in the VH alone.

We also investigated basal neurotransmission and excitability along the CA3 recurrent and the Schaffer collaterals-CA1 pathways in the VH. fEPSPs and population spikes (PS) recorded in CA3 and in CA1 to Schaffer collaterals stimulation were not significantly different in both genotypes (supplemental Fig. 3*A–E*, available at www.jneurosci.org as supplemental material). In addition, paired-pulse inhibition of PS (supplemental Fig. 3*F*, available at www.jneurosci.org as supplemental material) in CA1 did not differ in *GCLM* *-/-* and *+/+* mice. Thus, basal neurotransmission, excitability of pyramidal neurons and gross modulation of their excitability are not significantly altered in *GCLM* *-/-* mice. However, orthodromic PS in CA3 tended to be evoked at lower stimulus intensity and to reach higher amplitudes in *GCLM* *-/-* than in *+/+* mice (supplemental Fig. 3*C*, available at www.jneurosci.org as supplemental material). But the variability of orthodromic PS amplitude was particularly large in *GCLM* *-/-* mice. This could reflect a reduced perisomatic inhibition of some but not all pyramidal neurons in CA3 of *GCLM* *-/-* mice. Thus, these data indicate that the reduced β/γ oscillations in the VH of adult *GCLM* *-/-* mice are not associated with major and general impairments of neurotransmission and excitability.

Behavioral phenotype of *GCLM* *-/-* mice

Since *GCLM* *-/-* mice showed alteration in the GABAergic system specifically in the VH, we examined a series of hippocampus-dependent behaviors known in most cases to implicate differentially the VH and DH. These tests evaluated novelty-induced exploration, object recognition, spatial learning and memory, and behavioral responses to anxiety and fear-evoking situations. In a novel context, *GCLM* *-/-* mice were more active than *+/+* mice. When three objects were presented for the first time, *GCLM* *-/-* mice explored them more intensively than *+/+* mice did (Fig. 9*A*). After familiarization, the exploratory behavior of *GCLM* *-/-* mice dropped to sim-

ilar to *+/+* mice.

ilar levels than those of $+/+$ mice (supplemental Fig. 4A, available at www.jneurosci.org as supplemental material), indicating habituation to novelty after repeated exposures. When one of the three objects was moved to another location, both genotypes showed preference for the displaced object, but $GCLM^{-/-}$ mice spent more time exploring the non-displaced objects than $+/+$ mice did (Fig. 9B). When one of the previously non-displaced object was subsequently replaced by a novel object, $GCLM^{-/-}$ mice explored intensively both the novel object and the previously displaced object (Fig. 9C), suggesting an increased perseverative behavior. This could also reflect a difficulty of $GCLM^{-/-}$ mice to encode a novel object within a spatial context, requiring the mice to explore intensively the novel object and also the other objects. Thus, $GCLM^{-/-}$ mice recognize a spatially displaced object, but show altered behavior during an object recognition task.

We then examined spatial learning and memory, known to depend on DH. In a T-maze rewarded alternation task, both genotypes learned equally well to enter the previously unvisited arm (Fig. 9D), indicating intact spatial working memory in $GCLM^{-/-}$ mice. We also examined spatial reference learning and memory in a water maze. $GCLM^{-/-}$ and $+/+$ mice had similar swim performance (33.5 ± 4.3 cm/s vs 27.8 ± 2.9 cm/s) and found equally well the hidden platform (Fig. 9E). During the probe trial when the platform was removed, mice of both genotypes displayed similar preference for the goal quadrant (Fig. 9F). When the platform was moved to another location, $GCLM^{-/-}$ and $+/+$ mice were equally able to relearn the new location (Fig. 9E). Thus, spatial working memory, spatial reference learning and memory, and spatial reversal learning are normal in $GCLM^{-/-}$ mice.

As the VH is part of pathways modulating emotion and stress-related behaviors, we assessed the behavioral responses of $GCLM^{-/-}$ mice in tests that elicit mild stress. $GCLM^{-/-}$ mice entered significantly more often the open arms of an elevated plus maze than $+/+$ mice did (Fig. 10A). In a light/dark box, $GCLM^{-/-}$ mice performed also significantly more transitions between the two compartments and spent more time in the light compartment than $+/+$ mice did (Fig. 10B). In a novelty-suppressed feeding test, in which mice usually hesitate to approach a piece of food in the middle of an open field, $GCLM^{-/-}$ mice tended to contact the food quicker than $+/+$ mice did (supplemental Fig. 4B, available at www.jneurosci.org as supplemental material). Thus, $GCLM^{-/-}$ mice display less stress-induced behavioral inhibition.

Finally, we studied delay fear conditioning known to implicate the VH. Both genotypes responded to electric shocks by displaying strong vocalization, high locomotion, and jumping behavior to escape the aversive stimulus. In addition, mice of both genotypes reduced their overall activity following repeated shock pre-

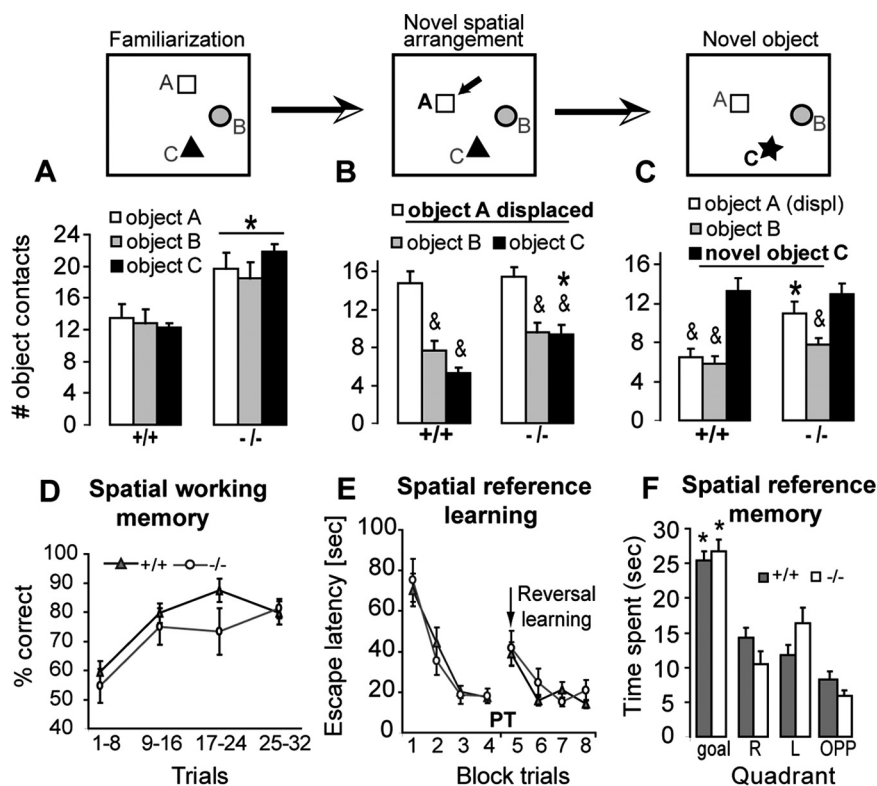


Figure 9. Object recognition (A–C) and spatial abilities (D–F) of $GCLM^{-/-}$ mice. **A**, During the first familiarization to 3 objects, $GCLM^{-/-}$ mice ($n = 12$) explore them more than $+/+$ mice do ($n = 14$) ($*p = 0.012$). **B**, Both genotypes show preference for the displaced object A ($*p < 0.001$), but $GCLM^{-/-}$ mice investigate more one of the non-displaced object (object C) than $+/+$ mice do ($*p = 0.002$). **C**, Novel object recognition is impaired in $GCLM^{-/-}$ mice ($p = 0.008$). When one of the non-displaced object (object C) is replaced by a novel object, $GCLM^{-/-}$ mice explore this novel object and the previously displaced object A with equal intensity. Exploration of the previously displaced object A remains higher in $GCLM^{-/-}$ than in $+/+$ mice ($*p = 0.01$). Only the familiar, non-displaced object (object B) is less investigated than the novel object by $GCLM^{-/-}$ mice ($*p = 0.004$). In contrast, $+/+$ mice explore more the novel object than the two familiar objects ($*p < 0.001$). **D**, Spatial working memory in a rewarded alternation task is intact in $GCLM^{-/-}$ mice. Percent of correct choice increases over the trial sessions similarly in $GCLM^{-/-}$ ($n = 8$) and $GCLM^{+/+}$ ($n = 8$) mice. **E**, Spatial reference learning in a water maze is intact in $GCLM^{-/-}$ mice. The ability to find a hidden platform (goal) improves equally well in $GCLM^{-/-}$ ($n = 6$) and $+/+$ ($n = 11$). After the platform was moved to another location (at the time indicated by an arrow), both genotypes learn equally well the new platform position. **F**, Spatial reference memory is intact in $GCLM^{-/-}$ mice. During the probe trial (PT), both genotypes spend more time in the goal quadrant than in the other quadrants ($*p \leq 0.003$). All data are presented with the mean \pm SEM.

sentation (Fig. 10C), suggesting that $GCLM^{-/-}$ mice have intact nociceptive sensory capacity. Though freezing increased with the number of received shocks in mice of both genotypes, $GCLM^{-/-}$ mice tended to freeze less than $+/+$ mice did (Fig. 10D). After conditioning, $GCLM^{-/-}$ mice froze significantly less when re-exposed to the context (Fig. 10E) or the tone (Fig. 10F) than $+/+$ mice did. Thus, $GCLM^{-/-}$ mice show reduced acquisition and expression of delay fear conditioning. Overall this shows that, compared to $+/+$ mice, $GCLM^{-/-}$ mice have intact spatial learning and spatial memory, but have increased novelty-induced exploration, altered behavior during an object recognition task, reduced behavioral inhibition under stress, and respond less to delay fear conditioning. This is consistent with a VH but not DH impairment.

Discussion

Our data underscore a selective vulnerability of the VH to redox dysregulation. A chronic GSH deficit causes elevated oxidative stress, specific reduction in PV-IR FSI and a concomitant reduction in β/γ oscillations in VH but not DH of young adult mice. The behavioral phenotype of $GCLM^{-/-}$ mice further corroborates a functional disruption of the VH but not DH. In addition to

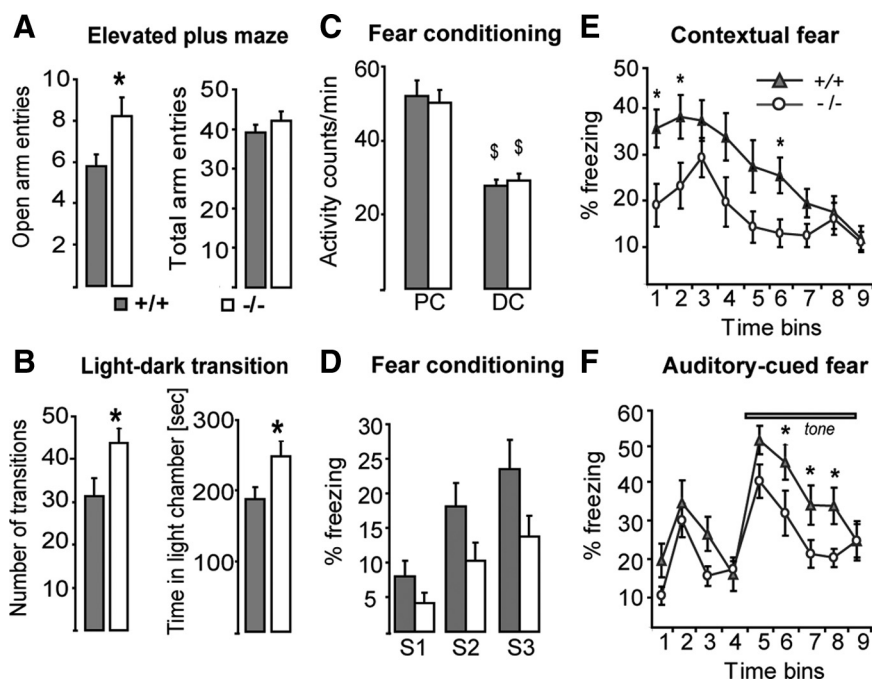


Figure 10. Behavioral responses of *GCLM* $-/-$ mice in mildly stressful and fearful conditions. **A**, In elevated plus maze, *GCLM* $-/-$ mice ($n = 13$) explore more frequently the open arms than *GCLM* $+/+$ mice do ($n = 25$) ($*p = 0.023$) (left panel). The total number of entries in both open and closed arms is not different in the two genotypes (right panel). **B**, In light/dark box, *GCLM* $-/-$ mice ($n = 7$) perform more transitions between the dark and light chamber than $+/+$ mice do ($n = 11$) ($*p = 0.045$) (left panel). *GCLM* $-/-$ mice spend more time in the light chamber than $+/+$ mice do ($*p = 0.027$) (right panel). **C**, Effect of delay fear conditioning on activity (number of crossings of infrared beams). Activity decreases during conditioning (DC), as compared to the preconditioning period (PC) ($^{\S}p < 0.001$). No difference between *GCLM* $-/-$ ($n = 11$) and $+/+$ mice ($n = 15$). **D**, Effects of consecutive shocks (S1–S3) on freezing. Freezing increases with the number of shocks ($p < 0.001$), but *GCLM* $-/-$ mice tend to freeze less than $+/+$ mice ($p = 0.054$). **E**, *GCLM* $-/-$ mice express less contextual fear conditioning than $+/+$ mice do ($p = 0.028$). *Significant difference between genotypes for a defined 1 min bin. **F**, *GCLM* $-/-$ mice express less auditory-cued fear conditioning than $+/+$ mice do ($p = 0.017$). *Significant difference between genotypes for a defined 1 min bin. Data are presented with the mean \pm SEM.

altered behavior during an object recognition task, *GCLM* $-/-$ mice display increased novelty-induced exploration, altered emotion and stress-related behaviors, but intact spatial learning and spatial memory.

As revealed by 8-Oxo-dG labeling, oxidative stress is present in VH but not DH of young adult *GCLM* $-/-$ mice, affecting mostly CA3 and DG where the reduction of PV-IR FSI is most severe. The elevated oxidative stress likely precedes the reduction of PV. In 20-d-old *GCLM* $-/-$ mice, the VH shows no oxidative stress and contains high density of PV-IR FSI. In 40-d-old *GCLM* $-/-$ mice, the VH (in particular CA3) presents signs of oxidative stress, but no yet significant deficit in PV-IR FSI. Thus, impairment of PV-IR FSI in VH of *GCLM* $-/-$ mice emerges after oxidative stress increases and/or cumulates throughout adolescence.

What could be responsible for the selective localization and timing of this oxidative stress? Its presence in VH but not in DH of adult *GCLM* $-/-$ mice is not due to lower GSH levels in the VH compared to DH. On the contrary, GSH levels are higher in VH, possibly as a response to increased ROS. It thus supports the concept that the oxidative stress in VH results from higher ROS production in VH compared to DH. The VH could be more vulnerable to redox dysregulation because of its richer catecholamine innervations compared to DH (Oleskevich et al., 1989; Gasbarri et al., 1997; Bjarkam et al., 2003). Auto-oxidation and catabolism of catecholamines form oxidative species including H_2O_2 , superoxide and o -quinones (Cadet and Brannock, 1998). Catecholamines react

also with cysteine residues of GSH and proteins to form conjugates in a superoxide-dependent manner (Rabinovic and Hastings, 1998; Hirrlinger et al., 2002). Furthermore, noradrenaline induces secretion of IL-6 by astrocytes (Maimone et al., 1993), as IL-6 is responsible (via a NOX-dependent superoxide overproduction) of PV impairment in ketamine-treated and aged rodents (Behrens et al., 2008; Dugan et al., 2009). Interestingly, noradrenergic innervations in VH are especially dense in CA3 and hilus of the DG (Oleskevich et al., 1989) and reach maximum density after weaning age (Moudy et al., 1993), coinciding in time and location with the oxidative stress observed in *GCLM* $-/-$ mice. Thus, a compromised GSH system might not cope with high levels of noradrenaline release in the ventral CA3 and DG, causing a regional oxidative stress.

PV-IR FSI require high-energy because of their fast-spiking properties and thus are likely to produce high amounts of ROS. These cells might be equipped to cope with such constraints. Thus, hippocampal PV-IR FSI have high levels of PGC-1 α (Cowell et al., 2007), which regulates metabolic demands in response to calcium flux and ATP levels, promotes survival under oxidative stress and enhances expression of Mn-superoxide dismutase, an antioxidant enzyme abundant in these FSI. Nevertheless, PV-IR FSI remain susceptible to excess of oxidative stress. Superoxide overproduction causes a decrease in GAD-67 and PV expression in a ketamine model of schizophrenia and a loss of PV FSI in aged mice (Behrens et al., 2007; Dugan et al., 2009). In addition, maturation and phenotypic maintenance of PV-IR FSI depend on calcium signaling via NR2A (Kinney et al., 2006), the redox-sensitive subunit of NMDAR (Choi et al., 2001), and L-type calcium channels (Jiang and Swann, 2005; Kinney et al., 2006). Redox dysregulation could impair PV-IR FSI via alteration of calcium signaling, since a GSH deficit causes hypofunction of NMDAR and alters dopamine modulation of calcium influx through L-type calcium channels (Steullet et al., 2006, 2008; Do et al., 2009a).

The deficit in PV-IR FSI has functional consequences. PV-IR FSI synapse on cell body and axonal initial segment of pyramidal cells, regulating their output and coordinating activity of neuronal assemblies. In hippocampal slices, kainate induces γ oscillations (Traub et al., 2004) dependent on recruitment of PV-IR FSI (Fuchs et al., 2007). We found that kainate-induced γ oscillations is decreased in VH but not DH of young adult *GCLM* $-/-$ mice, as is the density of PV-IR FSI. This suggests that a GSH deficit leads not merely to a reduction of PV expression but rather a profound functional disruption or even a decrease in number of these FSI in the VH. This is supported by the fact that kainate-induced γ oscillations are enhanced in mice that do not express PV in FSI (Vreugdenhil et al., 2003).

Using a series of hippocampus-dependent behaviors, we found that functional disruption of FSI in the VH contributes to

the behavioral phenotype of *GCLM* $-/-$ mice, although involvement of other potentially dysfunctional brain regions cannot be excluded. These mice display novelty-induced exploration, altered behavior during an object recognition task, altered emotion and stress-related behaviors, respond less to delay fear conditioning, but have intact spatial learning and spatial memory. It is worth comparing the *GCLM* $-/-$ behavioral phenotype to mice with reduced excitatory recruitment of PV-IR FSI in the whole hippocampus (Fuchs et al., 2007). Mice with functional disruption of PV-IR FSI in the whole hippocampus have deficit in recognition of novel spatial arrangement of familiar objects and in novel object recognition (Fuchs et al., 2007). In contrast, *GCLM* $-/-$ mice recognize changes in spatial arrangement of objects, a task that requires functional DH (Gaskin et al., 2009). Mice with functional disruption of PV-IR FSI in the whole hippocampus have also impaired spatial working memory (Fuchs et al., 2007) in a task dependent on the DH (McHugh et al., 2008; Gaskin et al., 2009), while *GCLM* $-/-$ mice do not show such deficit. The lack of spatial impairment in the *GCLM* $-/-$ mice indicates normal function of the DH (Bannerman et al., 2004; Broadbent et al., 2004). In addition, mice with functional disruption of PV-IR FSI in the entire hippocampus are hypoactive, while *GCLM* $-/-$ mice show strong novelty-induced exploration. Such hyperactivity can be induced by a decreased GABA inhibition in the VH (Bast et al., 2001a). The altered behavior of *GCLM* $-/-$ mice under mild stress (in elevated plus maze and light/dark box) is also in line with a specific functional disruption of the VH but not DH (Bannerman et al., 2004). Finally, the reduced expression of fear delay conditioning in *GCLM* $-/-$ mice suggests alteration of information processing in the VH. The VH is indeed implicated in both contextual and auditory-cued delay fear conditioning, while the DH is involved in trace fear conditioning and contextual delay fear conditioning (Bast et al., 2001b, Hunsaker and Kesner, 2008, Esclassan et al., 2009). In particular, lesions of the ventral CA3 causes deficit in expression of both auditory-cued and contextual delay fear conditioning (Hunsaker and Kesner, 2008). Together, chronic GSH deficit impacts the structural and functional integrity of PV-IR FSI, impairing information processing in the VH and leading to specific changes in behaviors such as enhanced novelty-induced exploration, inadequate responses to stress and impaired responses to fear.

The finding that the VH is particularly susceptible to oxidative stress is also of interest in regard to schizophrenia. There is growing evidence of structural and functional anomalies of the anterior hippocampus (VH in rodents) in schizophrenia patients (Goldman and Mitchell, 2004). This includes elevated blood flow at rest and reduced activation during specific tasks (Jessen et al., 2003; Ongur et al., 2006). The projections from the ventral/anterior hippocampus to the PFC, the modulation by the ventral/anterior hippocampus of dopamine release in the PFC and nucleus accumbens, and the schizophrenia-like anomalies induced by neonatal lesion of the VH in rats further suggest a significant role of the anterior hippocampus in the pathology of schizophrenia (Goldman and Mitchell, 2004).

A marked reduction of PV-IR FSI density is described in the middle hippocampus of schizophrenia and bipolar patients (Zhang and Reynolds, 2002). In both disorders, the GABAergic system is mostly affected in the CA3/2 region as revealed by GAD-67 expression (Benes et al., 2007). To our knowledge however, there is no data on anomalies of the GABAergic system along the longitudinal axis of patient's hippocampus. Decreased PV expression or abnormal maturation of FSI are observed in experimental animal models for schizophrenia (Penschuck et al.,

2006; Behrens et al., 2007; Tseng et al., 2008; Lodge et al., 2009), and following environmental factors (Dell'Anna et al., 1996; Harte et al., 2007; Meyer et al., 2008) or manipulations of genes associated with schizophrenia (Hikida et al., 2007; Shen et al., 2008; Fisahn et al., 2009). However, the degree of PV impairment and the susceptible brain structures vary across models and depend on the time of manipulation. Thus, prenatal immune challenge at E9 affects PV in the PFC, while similar insult at E17 impacts PV in both PFC and VH (Meyer et al., 2008). Likewise, blockade of NMDAR at prenatal, postnatal, adolescent or adult age does not impact PV-IR FSI in the same way and same brain structures (Abekawa et al., 2007; Wang et al., 2008; Zhang et al., 2008). A GSH deficit has also region- and time-specific effects on PV-IR FSI, causing reduction of PV-IR FSI in the VH of adults but affecting also postnatal maturation of PV FSI in the anterior cingulate cortex (Cabungcal et al., 2006; Do et al., 2009a). Thus, impairment of PV-IR FSI could be quite heterogeneous among patients depending on their genetic background and the nature and time of various risk factor impacts (Jaaro-Peled et al., 2009). Therefore, examination within the same subjects of FSI in the different subregions of the PFC and hippocampus might reveal different endophenotypes.

In summary, a redox dysregulation induced by a compromised GSH synthesis leads to region and time selective oxidative stress and impairment of the structural and functional integrity of FSI. Interestingly, FSI defects in the VH appear toward end of adolescence/early adulthood, a period during which symptoms of schizophrenia emerges. This demonstrates that redox dysregulation from a genetic origin and/or induced by environmental risk factors (infections, stress) could be central to the development of psychiatric disorders, including schizophrenia.

References

- Abekawa T, Ito K, Nakagawa S, Koyama T (2007) Prenatal exposure to an NMDA receptor antagonist, MK-801 reduces density of parvalbumin-immunoreactive GABAergic neurons in the medial prefrontal cortex and enhances phencyclidine-induced hyperlocomotion but not behavioral sensitization to methamphetamine in postpubertal rats. *Psychopharmacology (Berl)* 192:303–316.
- Bannerman DM, Rawlins JN, McHugh SB, Deacon RM, Yee BK, Bast T, Zhang WN, Pothuizen HH, Feldon J (2004) Regional dissociations within the hippocampus—memory and anxiety. *Neurosci Biobehav Rev* 28:273–283.
- Bartos M, Vida I, Jonas P (2007) Synaptic mechanisms of synchronized gamma oscillations in inhibitory interneuron networks. *Nat Rev Neurosci* 8:45–56.
- Bast T, Zhang WN, Feldon J (2001a) Hyperactivity, decreased startle reactivity, and disrupted prepulse inhibition following disinhibition of the rat ventral hippocampus by the GABA(A) receptor antagonist picrotoxin. *Psychopharmacology (Berl)* 156:225–233.
- Bast T, Zhang WN, Feldon J (2001b) The ventral hippocampus and fear conditioning in rats. Different anterograde amnesias of fear after tetrodotoxin inactivation and infusion of the GABA(A) agonist muscimol. *Exp Brain Res* 139:39–52.
- Behrens MM, Ali SS, Dao DN, Lucero J, Shekhtman G, Quick KL, Dugan LL (2007) Ketamine-induced loss of phenotype of fast-spiking interneurons is mediated by NADPH-oxidase. *Science* 318:1645–1647.
- Behrens MM, Ali SS, Dugan LL (2008) Interleukin-6 mediates the increase in NADPH-oxidase in the ketamine model of schizophrenia. *J Neurosci* 28:13957–13966.
- Benes FM, Lim B, Matzilevich D, Walsh JP, Subburaju S, Minns M (2007) Regulation of the GABA cell phenotype in hippocampus of schizophrenics and bipolars. *Proc Natl Acad Sci U S A* 104:10164–10169.
- Bjarkam CR, Sorensen JC, Geneser FA (2003) Distribution and morphology of serotonin-immunoreactive axons in the hippocampal region of the New Zealand white rabbit. I. Area dentata and hippocampus. *Hippocampus* 13:21–37.
- Broadbent NJ, Squire LR, Clark RE (2004) Spatial memory, recognition

- memory, and the hippocampus. *Proc Natl Acad Sci U S A* 101:14515–14520.
- Cabungcal JH, Nicolas D, Kraftsik R, Cuenod M, Do KQ, Hornung JP (2006) Glutathione deficit during development induces anomalies in the rat anterior cingulate GABAergic neurons: relevance to schizophrenia. *Neurobiol Dis* 22:624–637.
- Cadet JL, Brannock C (1998) Free radicals and the pathobiology of brain dopamine systems. *Neurochem Int* 32:117–131.
- Cho RY, Konecky RO, Carter CS (2006) Impairments in frontal cortical gamma synchrony and cognitive control in schizophrenia. *Proc Natl Acad Sci U S A* 103:19878–19883.
- Choi Y, Chen HV, Lipton SA (2001) Three pairs of cysteine residues mediate both Redox and Zn²⁺ modulation of the NMDA receptor. *J Neurosci* 21:392–400.
- Cowell RM, Blake KR, Russell JW (2007) Localization of the transcriptional coactivator PGC-1alpha to GABAergic neurons during maturation of the rat brain. *J Comp Neurol* 502:1–18.
- Dell'Anna E, Geloso MC, Magarelli M, Molinari M (1996) Development of GABA and calcium binding proteins immunoreactivity in the rat hippocampus following neonatal anoxia. *Neurosci Lett* 211:93–96.
- Do KQ, Trabesinger AH, Kirsten-Kruger M, Lauer CJ, Dydak D, Hell D, Holsboer F, Boesiger P, Cuenod M (2000) Schizophrenia: glutathione deficit in cerebrospinal fluid and prefrontal cortex in vivo. *Eur J Neurosci* 12:3721–3728.
- Do KQ, Cabungcal JH, Frank A, Steullet P, Cuenod M (2009a) Redox dysregulation, neurodevelopment and schizophrenia. *Curr Opin Neurobiol* 19:220–230.
- Do KQ, Bovet P, Cabungcal JH, Conus P, Gysin R, Lavoie S, Steullet P, Cuenod M (2009b) Redox dysregulation in schizophrenia: genetic susceptibility and pathophysiological mechanisms. In: *Handbook of neurochemistry and molecular neurobiology: schizophrenia*, Vol 27, Ed 3, (Javitt DC, Kantrowitz JT, Lajtha A, eds), pp 285–311. New York: Springer.
- Dugan LL, Ali SS, Shekhtman G, Roberts AJ, Lucero J, Quick KL, Behrens MM (2009) IL-6 mediated degeneration of forebrain GABAergic interneurons and cognitive impairment in aged mice through activation of neuronal NADPH oxidase. *PLoS One* 4:e518.
- Esclassan F, Coutureau E, Di SG, Marchand AR (2009) Differential contribution of dorsal and ventral hippocampus to trace and delay fear conditioning. *Hippocampus* 19:33–44.
- Fisahn A, Neddens J, Yan L, Buonanno A (2009) Neuregulin-1 modulates hippocampal gamma oscillations: implications for schizophrenia. *Cereb Cortex* 19:612–618.
- Fries P, Nikolic D, Singer W (2007) The gamma cycle. *Trends Neurosci* 30:309–316.
- Fuchs EC, Zivkovic AR, Cunningham MO, Middleton S, Lebeau FE, Bannerman DM, Rozov A, Whittington MA, Traub RD, Rawlins JN, Monyer H (2007) Recruitment of parvalbumin-positive interneurons determines hippocampal function and associated behavior. *Neuron* 53:591–604.
- Gasbarri A, Sulli A, Packard MG (1997) The dopaminergic mesencephalic projections to the hippocampal formation in the rat. *Prog Neuropharmacol Biol Psychiatry* 21:1–22.
- Gaskin S, Gamliel A, Tardif M, Cole E, Mumby DG (2009) Incidental (unreinforced) and reinforced spatial learning in rats with ventral and dorsal lesions of hippocampus. *Behav Brain Res* 202:64–70.
- Goldman MB, Mitchell CP (2004) What is the functional significance of hippocampal pathology in schizophrenia? *Schizophr Bull* 30:367–392.
- Gysin R, Kraftsik R, Sandell J, Bovet P, Chappuis C, Conus P, Deppen P, Preisig M, Ruiz V, Steullet P, Tosic M, Werge T, Cuénod M, Do KQ (2007) Impaired glutathione synthesis in schizophrenia: convergent genetic and functional evidence. *Proc Natl Acad Sci U S A* 104:16621–16626.
- Harte MK, Powell SB, Swerdlow NR, Geyer MA, Reynolds GP (2007) Deficits in parvalbumin and calbindin immunoreactive cells in the hippocampus of isolation reared rats. *J Neural Transm* 114:893–898.
- Hashimoto T, Volk DW, Eggen SM, Mirnics K, Pierri JN, Sun Z, Sampson AR, Lewis DA (2003) Gene expression deficits in a subclass of GABA neurons in the prefrontal cortex of subjects with schizophrenia. *J Neurosci* 23:6315–6326.
- Hikida T, Jaaro-Peled H, Seshadri S, Oishi K, Hookway C, Kong S, Wu D, Xue R, Andrade M, Tankou S, Mori S, Gallagher M, Ishizuka K, Pletnikov M, Kida S, Sawa A (2007) Dominant-negative DISC1 transgenic mice display schizophrenia-associated phenotypes detected by measures translatable to humans. *Proc Natl Acad Sci U S A* 104:14501–14506.
- Hirrlinger J, Schulz JB, Dringen R (2002) Effects of dopamine on the glutathione metabolism of cultured astroglial cells: implications for Parkinson's disease. *J Neurochem* 82:458–467.
- Hunsaker MR, Kesner RP (2008) Dissociations across the dorsal-ventral axis of CA3 and CA1 for encoding and retrieval of contextual and auditory-cued fear. *Neurobiol Learn Mem* 89:61–69.
- Jaaro-Peled H, Hayashi-Takagi A, Seshadri S, Kamiya A, Brandon NJ, Sawa A (2009) Neurodevelopmental mechanisms of schizophrenia: understanding disturbed postnatal brain maturation through neuregulin-1-ErbB4 and DISC1. *Trends Neurosci* 32:485–495.
- Jessen F, Scheef L, Germeshausen L, Tawo Y, Kockler M, Kuhn KU, Maier W, Schild HH, Heun R (2003) Reduced hippocampal activation during encoding and recognition of words in schizophrenia patients. *Am J Psychiatry* 160:1305–1312.
- Jiang M, Swann JW (2005) A role for L-type calcium channels in the maturation of parvalbumin-containing hippocampal interneurons. *Neuroscience* 135:839–850.
- Kasai H (1997) Analysis of a form of oxidative DNA damage, 8-hydroxy-2'-deoxyguanosine, as a marker of cellular oxidative stress during carcinogenesis. *Mutat Res* 387:147–163.
- Kinney JW, Davis CN, Tabarean I, Conti B, Bartfai T, Behrens MM (2006) A specific role for NR2A-containing NMDA receptors in the maintenance of parvalbumin and GAD67 immunoreactivity in cultured interneurons. *J Neurosci* 26:1604–1615.
- Lewis DA, Hashimoto T, Volk DW (2005) Cortical inhibitory neurons and schizophrenia. *Nat Rev Neurosci* 6:312–324.
- Lodge DJ, Behrens MM, Grace AA (2009) A loss of parvalbumin-containing interneurons is associated with diminished oscillatory activity in an animal model of schizophrenia. *J Neurosci* 29:2344–2354.
- Maimone D, Cioni C, Rosa S, Macchia G, Aloisi F, Annunziata P (1993) Norepinephrine and vasoactive intestinal peptide induce IL-6 secretion by astrocytes: synergism with IL-1 beta and TNF alpha. *J Neuroimmunol* 47:73–81.
- McHugh SB, Niewoehner B, Rawlins JN, Bannerman DM (2008) Dorsal hippocampal N-methyl-D-aspartate receptors underlie spatial working memory performance during non-matching to place testing on the T-maze. *Behav Brain Res* 186:41–47.
- Meyer U, Nyffeler M, Yee BK, Knuesel I, Feldon J (2008) Adult brain and behavioral pathological markers of prenatal immune challenge during early/middle and late fetal development in mice. *Brain Behav Immun* 22:469–486.
- Moudy AM, Kunkel DD, Schwartzkroin PA (1993) Development of dopamine-beta-hydroxylase-positive fiber innervation of the rat hippocampus. *Synapse* 15:307–318.
- Oleskevich S, Descarries L, Lacaille JC (1989) Quantified distribution of the noradrenaline innervation in the hippocampus of adult rat. *J Neurosci* 9:3803–3815.
- Ongur D, Cullen TJ, Wolf DH, Rohan M, Barreira P, Zalesak M, Heckers S (2006) The neural basis of relational memory deficits in schizophrenia. *Arch Gen Psychiatry* 63:356–365.
- Penschuck S, Flagstad P, Didriksen M, Leist M, Michael-Titus AT (2006) Decrease in parvalbumin-expressing neurons in the hippocampus and increased phencyclidine-induced locomotor activity in the rat methylazoxymethanol (MAM) model of schizophrenia. *Eur J Neurosci* 23:279–284.
- Rabinovic AD, Hastings TG (1998) Role of endogenous glutathione in the oxidation of dopamine. *J Neurochem* 71:2071–2078.
- Schmitz C, Hof PR (2005) Design-based stereology in neuroscience. *Neuroscience* 130:813–831.
- Shen S, Lang B, Nakamoto C, Zhang F, Pu J, Kuan SL, Chatzi C, He S, Mackie I, Brandon NJ, Marquis KL, Day M, Hurko O, McCaig CD, Riedel G, St Clair D (2008) Schizophrenia-related neural and behavioral phenotypes in transgenic mice expressing truncated *Disc1*. *J Neurosci* 28:10893–10904.
- Sohal VS, Zhang F, Yizhar O, Deisseroth K (2009) Parvalbumin neurons and gamma rhythms enhance cortical circuit performance. *Nature* 459:698–702.
- Steullet P, Neijt HC, Cuenod M, Do KQ (2006) Synaptic plasticity impairment and hypofunction of NMDA receptors induced by glutathione deficit: relevance to schizophrenia. *Neuroscience* 137:807–819.

- Steullet P, Lavoie S, Kraftsik R, Guidi R, Gysin R, Cuenod M, Do KQ (2008) A glutathione deficit alters dopamine modulation of L-type calcium channels via D2 and ryanodine receptors in neurons. *Free Radic Biol Med* 44:1042–1054.
- Tosic M, Ott J, Barral S, Bovet P, Deppen P, Gheorghita F, Matthey ML, Parnas J, Preisig M, Saraga M, Solida A, Timm S, Wang AG, Werge T, Cuenod M, Do KQ (2006) Schizophrenia and oxidative stress: glutamate cysteine ligase modifier as a susceptibility gene. *Am J Hum Genet* 79:586–592.
- Traub RD, Bibbig A, Lebeau FE, Buhl EH, Whittington MA (2004) Cellular mechanisms of neuronal population oscillations in the hippocampus in vitro. *Annu Rev Neurosci* 27:247–278.
- Tseng KY, Lewis BL, Hashimoto T, Sesack SR, Kloc M, Lewis DA, O'Donnell P (2008) A neonatal ventral hippocampal lesion causes functional deficits in adult prefrontal cortical interneurons. *J Neurosci* 28:12691–12699.
- Uhlhaas PJ, Haenschel C, Nikolic D, Singer W (2008) The role of oscillations and synchrony in cortical networks and their putative relevance for the pathophysiology of schizophrenia. *Schizophr Bull* 34:927–943.
- Valko M, Leibfritz D, Moncol J, Cronin MT, Mazur M, Telser J (2007) Free radicals and antioxidants in normal physiological functions and human disease. *Int J Biochem Cell Biol* 39:44–84.
- Vreugdenhil M, Jefferys JG, Celio MR, Schwaller B (2003) Parvalbumin-deficiency facilitates repetitive IPSCs and gamma oscillations in the hippocampus. *J Neurophysiol* 89:1414–1422.
- Wang CZ, Yang SF, Xia Y, Johnson KM (2008) Postnatal phencyclidine administration selectively reduces adult cortical parvalbumin-containing interneurons. *Neuropsychopharmacology* 33:2442–2455.
- West MJ (1999) Stereological methods for estimating the total number of neurons and synapses: issues of precision and bias. *Trends Neurosci* 22:51–61.
- West MJ (2002) Design-based stereological methods for counting neurons. *Prog Brain Res* 35:43–51.
- West MJ, Slomianka L, Gundersen HJ (1991) Unbiased stereological estimation of the total number of neurons in the subdivisions of the rat hippocampus using optical fractionator. *Anat Rec* 231:482–497.
- Yang Y, Dieter MZ, Chen Y, Shertzer HG, Nebert DW, Dalton TP (2002) Initial characterization of the glutamate-cysteine ligase modifier subunit Gclm(–/–) knockout mouse. Novel model system for a severely compromised oxidative stress response. *J Biol Chem* 277:49446–49452.
- Zhang Y, Behrens MM, Lisman JE (2008) Prolonged exposure to NMDAR antagonist suppresses inhibitory synaptic transmission in prefrontal cortex. *J Neurophysiol* 100:959–965.
- Zhang ZJ, Reynolds GP (2002) A selective decrease in the relative density of parvalbumin-immunoreactive neurons in the hippocampus in schizophrenia. *Schizophr Res* 55:1–10.